Supplementary Material

Challenges of today for Na-based batteries of the future: from materials to cell metrics

Ivana Hasa[a,b,c], Sathiya Mariyappan[d,e,f], Damien Saurel[g,f], Philipp Adelhelm[,h,i], Alexey Y. Koposov[j], Christian Masquelier[k,e,f], Laurence Croguennec[l,e,f], Montse Casas-Cabanas*[g,f,m]

[a] WMG, The University of Warwick, Coventry CV4 7AL, United Kingdom

[b] Helmholtz Institute Ulm (HIU), Helmholtzstrasse 11, 89081 Ulm, Germany

[c] Karlsruhe Institute of Technology (KIT), P.O. Box 3640, 76021 Karlsruhe, Germany

[d] Chimie du Solide-Energie, UMR 8260, Collège de France, 75231 Paris Cedex 05, France

[e] Réseau sur le Stockage Electrochimique de l'Energie (RS2E), FR CNRS 3459, Amiens, France

[f] ALISTORE-European Research Institute, 80039 Amiens, France

[g] Center for Cooperative Research on Alternative Energies (CIC energiGUNE), Basque Research and Technology Alliance (BRTA), Parque Tecnológico de Alava, Albert Einstein 48, 01510, Vitoria-Gasteiz, Spain

[h] Institute of Chemistry, Humboldt-University Berlin, Brook-Taylor-Str. 2, Berlin, Germany

[i] Helmholtz-Zentrum Berlin für Materialien und Energy, Albert-Einstein-Str. 15 12489 Berlin, Germany

[j] Department of Battery Technology, Institute for Energy Technology (IFE), Instituttveien 18, NO-2007 Kjeller, Norway

[k] Laboratoire de Réactivité et Chimie des Solides, UMR CNRS #7314, Université de Picardie Jules Verne, 80039 Amiens Cedex, France

[l] CNRS, Univ. Bordeaux, Bordeaux INP, ICMCB, UMR CNRS 5026, F-33600 Pessac, France

[m] Ikerbasque, Basque Foundation for Science, María Díaz de Haro 3, 48013, Bilbao, Spain

Corresponding author: mcasas@cicenergigune.com

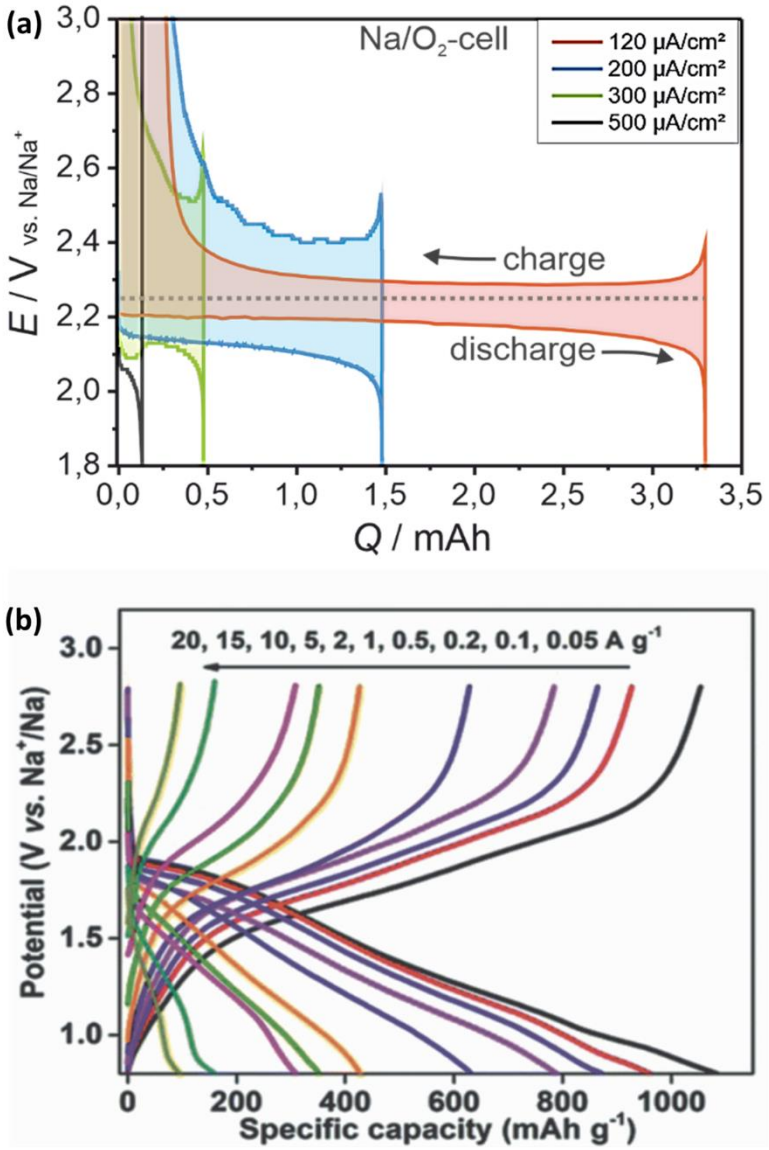

Figure 7

Figure S1: (a) Voltage profiles of a Na/O_2 cell with NaO_2 as discharge product at different current densities. Reprinted and adapted from [1] with permission from Springer Nature Copyright © (2012). (b) Voltage profiles of a Na/S cell at different current densities. Reprinted and adapted from [2] with permission from The Royal Society of Chemistry Copyright © (2020).

Table S1: Practical capacity and capacity retention of a selection of best reported Na-ion full cells, compared to reported $LiCoO_2$-graphite Li-ion full cell as a reference.

No	Material (positive-negative)	Q_{theo} (mAh/g)	Electrolyte	Cell details	Experimental conditions	Q_{pra} (mAh/g) / no. of cycles / retention (%)	Ref
1.	O3 $NaNi_{0.5}Mn_{0.5}O_2$ - Hard carbon	240	1M $NaPF_6$ in PC	Coin type R2032	1.7 - 3.8 V	125 /100 / ~80	[3]
					1.2 - 4.2 V	190 / 50 / ~50	
2.	O3 $NaNi_{1-x-y}Mn_xTi_yO_2$ - Hard carbon	~240-250	1M $NaPF_6$ in PC	Coin type R2032	1.2 - 4 V	120 / 100 / >80	
					1.2 - 4.4 V	190 / 50 / >60	
3.	O3 $NaNi_{0.68}Mn_{0.22}Co_{0.10}O_2$ - hard carbon	~240	1.2 M NaFSI in DME-BTFE	Coin type R2032	1.2 - 4.1 V	188 / 200 / 80	[4]
					1.2 - 3.9 V	137 / 1000 / 81	
				Pouch cells	1.2 - 4.1 V	184 / 100 / 83	
					1.2 - 3.9 V	141 / 450 / 82	
4.	O3 $NaCu_{0.2}(Fe_{1/3}Mn_{2/3})_{0.8}O_2$ - Alloy type P-TiP2-C	~240	1 M $NaClO_4$ in PC- FEC (98:2)	Coin type cells	1.2 - 4.2 V	130 / 100 / ~40	[5]
5.	P2 $Na_{0.6}Ni_{0.22}Fe_{0.11}Mn_{0.66}O_2$ - Sb-C alloy	160 (for 0.6 Na)	1 M $NaClO_4$ in PC-FEC (8 : 2 W/W)	Swagelok T-type cell	0.7 - 4.1 V	120 / 15 / ~90	[6]
6.	O3 or O3-P2 mixture of $Na_aNi_{(1-x-y-z)}Mn_xMg_yTi_zO_2$ - Hard carbon	~240	0.5 $NaPF_6$ in organic carbonates	Pouch type	1 - 4.3 V (C/2 rate)	~150 / >80% retention claimed after 400 cycles based on linear extrapolation	[7]
7.	O3 $NaNi_{0.45}Zn_{0.05}Mn_{0.4}Ti_{0.1}O_2$ - Hard carbon	~240	1M $NaPF_6$ in PC	Coin type R2032	1.2 - 4.4 V	170 / 100 / 83	Own results
8.	O3 $NaNi_{0.12}Cu_{0.12}Mg_{0.12}Fe_{0.15}Co_{0.15}Mn_{0.1}Ti_{0.1}Sn_{0.1}Sb_{0.04}O_2$ - Hard carbon	~230	1 M $NaClO_4$ in EC-PC-DMC (1: 1: 1) + 2 wt% FEC as additive	Coin type CR2032 cells	0.5 - 3.9 V	~300 (based on hard carbon weight) / 100 / 88.5	[8]
9.	O3 $Na_xNi_{1/3}Fe_{1/3}Mn_{1/3}O_2$ - hard carbon	~240	1M $NaPF_6$ in EC-EMC (1: 1)+ 2 wt% FEC	Pouch cell	2 - 3.9 V	~120 / 100 / 93	[9]

10.	O3-type $Na[Li_{0.05}Mn_{0.50}Ni_{0.30}Cu_{0.10}Mg_{0.05}]O_2$ - Hard carbon	250	1 M $NaClO_4$ in EC-DMC (1 : 1) + 2 wt% FEC	R2032 coin type	1 - 4 V	172 / 200 / 88	[10]
11.	P2 $Na_{0.67}Mg_{0.3}Mn_{0.7}O_2$	190 (for 0.67 Na)	1M $NaPF_6$ in PC	Coin type R2032	1.5 - 4.5 V	130 / 100 / >85	[3]
12.	P2 $Na_{0.67}(Fe_{0.5}Mn_{0.5})O_2$	175 (for 0.67 Na)	1M $NaPF_6$ in PC	Coin type R2032	1.5 - 4.2 V	100 / 100 / > 85	
13.	$Na_3V_2(PO_4)_2F_3$ - hard carbon	~180 (for 3Na)	1 M $NaPF_6$ in EC-DMC (1:1)	18650 cylindrical cells	2 - 4.25 V	~100 (2 Na used) / 4000 / 80	[11]
14.	$Na_xMnFe(CN)_6$ - Hard carbon	~160 (for 2 Na)	Undisclosed	Pouch type	1.5 - 3.5 V	~100 / 500 / >95	[7]
15.	$LiCoO_2$- Graphite	~270 (for 1 Li)	1M $LiPF_6$ EC-DMC	Pouch type	2.75- 4.2 V (depends on the SOC used)	> 90% retention after 500 cycles	[12]

Table S2: Redox couple, average discharge voltage, theoretical capacity, theoretical energy density and reported practical capacity in half cell of a selection of the best polyanionic positive electrode materials.

Material	Redox couple	Average discharge voltage (V vs. Na)	Theoretical capacity (mAh/g)	Theoretical energy density (Wh/kg)	Practical capacity (mAh/g) / Rate capability when available
$NaFePO_4$	Fe^{3+}/Fe^{2+}	2.7	154	462	100 mAh/g at C/10 after 240 cycles (1 Na^+ exchanged per f.u. in the potential window 2 - 3.8 V vs Na) [13]
$Na_2FeP_2O_7$	Fe^{3+}/Fe^{2+}	2.9	97	282	< 90 mAh/g at 1C after 60 cycles (1 Na^+ exchanged per f.u. in the potential range 2 - 4 V vs Na) [14]
$Na_4(Fe,Mn)_3(PO_4)_2(P_2O_7)$	Fe^{3+}/Fe^{2+}, Mn^{3+}/Mn^{2+}	3.0	129	387	< 50 mAh/g at 10C over 6000 cycles (3 Na^+ exchanged per f.u. in the potential range 1.7 – 4.3 V vs Na) [15]
$Na_{2+2x}Fe_{2-x}(SO_4)_3$	Fe^{3+}/Fe^{2+}	3.8	134	509	~ 70 mAh/g at 10C after 500 cycles (2 Na^+ exchanged per f.u.) in the potential range 2 – 4.5 V vs Na [16]
Na_2MnSiO_4	Mn^{3+}/Mn^{2+}	3.2	139 (for 1 Na^+ exchanged)	445	~140 mAh/g at 1C over 500 cycles (1 Na^+ exchanged per f.u. in the potential window 2 - 4.3 V vs Na with a 2h constant voltage at 4.3 V for each end of charge) [17]
$Na_3V_2(PO_4)_3$	V^{4+}/V^{3+}	3.4	118	401	~100 mAh/g at C/10 over 80 cycles (2 Na^+ exchanged per f.u. in the potential window 2.7 - 3.7 vs. Na) [18]
$Na_3V_2(PO_4)_2F_3$	V^{4+}/V^{3+}	3.9	129	499	~100 mAh/g at 1C over 4000 cycles (2 Na^+ exchanged per f.u. in the potential window 2 - 4.3 V vs. Hard Carbon), up to 30C with 80% capacity retention [9]

Method for the calculation of energy densities at cell level:

For the cell design, 1 cm thick prismatic pouch cell has been chosen as industrial standard, with double sided coatings except for the outer layers (negative electrodes).[19,20] The porosity of all electrode coatings has been set to 30%. The thickness of positive electrodes has been fixed to 65 µm as industrial standard,[21] and the negative electrode thickness has been adjusted to ensure a 1:1 capacity balance. The number of stacks is then dependent on the negative electrode coating thickness (which depends on the negative electrode's active material capacity and density), and it has been adjusted to get the closest to a total nude cell thickness of 1cm. The composition of all electrodes has been set to 90:5:5 in active material, binder and conductive carbon additive, respectively. 10 µm copper foil has been considered for the negative electrode of Li-ion cells, and 15µm aluminum foil has been considered for all other electrodes (positive electrodes of Li-ion cells and both electrodes of Na-ion cells), which lie within the range of thickness used in the present commercial Li-ion cells.[20,22] For the separator, Celgard A273 monolayer polypropylene has been selected, with a thickness of 16 µm and a porosity of 40% according to the manufacturer specifications, which lie within the range of values reported by e.g. Lain et al. for a series of commercial Li-ion cells.[22]For the electrolyte, $LiPF_6$ or $NaPF_6$ 1M in EC:DMC 1:1 has been chosen, whose volume has been calculated so as to fill the porosity of the electrodes (30 %) and separator (40%). The values of the parameters for all cell components and materials used for the calculations are presented in tables S3-5.

The specific energy and energy density values, E_G and E_V, respectivelly, presented in table S6, have been calculated on the basis of the cell volume and the weight of all cell components, but not taking into account the pouch envelop nor the contact tabs, according to the following expressions:

$$E_G(Wh.kg^{-1}) = \frac{Q_+(E_+ - E_-)}{m_{cell}}$$

$$E_V(Wh.kg^{-1}) = E_G \frac{m_{cell}}{V_{cell}}$$

where Q_+ and E_+ are the capacity and average oxidation potential of the positive electrode active material, and E_- the average reduction potential of the negative electrode active material; m_{cell} and V_{cell} are the total weight and volume of all cell components, respectively, except pouch envelop and contact tabs:

$$m_{cell} = m_{AM} + m_{binder} + m_{CB} + m_{foils} + m_{electrolyte} + m_{sep}$$

$$V_{cell} = A \cdot e_{cell}$$

where A is the electrode area (same for all Li-ion and Na-ion electrodes) and e_{cell} the total cell thickness.

The total active material weight m_{AM} is calculated as follows, for positive (m_{AM+}) and negative (m_{AM-}) electrodes:

$$m_{AM} = m_{AM+} + m_{AM-}$$

$$m_{AM+} = A \cdot e_+ \cdot C_{AM+} \cdot (1 - P) \cdot d_{AM+} \cdot n$$

$$m_{AM-} = A \cdot e_- \cdot C_{AM-} \cdot (1 - P) \cdot d_{AM-} \cdot n$$

where C_{AM} is the weight percentage of active material within the coating (C_{AM} = 90% for all electrodes of all Li-ion and Na-ion cells), P the coating porosity (30% in volume for all electrodes of all Li-ion and Na-ion cells), d_{AM} the theoretical density of active material and n the number of positive-negative electrodes stacks.

The coating thickness e_- of the negative electrode is adjusted so that its areal capacity equals that of the positive electrode:

$$e_- = e_+ \frac{Q_+}{Q_-} \frac{d_+}{d_-}$$

where e_+ is the coating thickness of the positive electrode (65 m), Q_+ and Q_- are the specific capacities of the active materials of the positive and negative electrodes, respectively, and d_+ and d_- are the theoretical densities of the active materials of the positive and negative electrodes, respectively.

The total binder's weight m_{binder} is calculated as follows, for each electrode:

$$m_{binder} = m_{binder+} + m_{binder-}$$

$$m_{binder+} = A \cdot e_+ \cdot C_B \cdot (1 - P) \cdot d_B \cdot n$$

$$m_{binder-} = A \cdot e_- \cdot C_B \cdot (1 - P) \cdot d_B \cdot n$$

where C_B is the weight percentage of binder within the coating (C_B = 5% for all electrodes of all Li-ion and Na-ion cells) and d_B the binder's density.

The carbon black's weight m_{CB} is calculated as follows, for each electrode:

$$m_{CB} = m_{CB+} + m_{CB-}$$

$$m_{CB+} = A \cdot e_+ \cdot C_{CB} \cdot (1 - P) \cdot d_{CB} \cdot n$$

$$m_{CB-} = A \cdot e_- \cdot C_{CB} \cdot (1 - P) \cdot d_{CB} \cdot n$$

where C_{CB} is the weight percentage of carbon black within the coating (C_{CB} = 5% for all electrodes of all Li-ion and Na-ion cells), P the coating porosity (30% in volume for all electrodes of all Li-ion and Na-ion cells) and d_{CB} the carbon black's density.

The positive electrode foil weight m_{foil+} is calculated as follows:

$$m_{foil+} = A \cdot e_{foil+} \cdot d_{foil+} \cdot \frac{n}{2}$$

where e_{foil+} is the aluminum foil thickness (10 mm) and d_{foil+} its density. The factor ½ is due to the fact that the foils are coated on both sides.

The negative electrode foil weight m_{foil-} is calculated as follows:

$$m_{foil-} = A \cdot e_{foil-} \cdot d_{foil-} \cdot \left(\frac{n}{2} + 1\right)$$

where e_{foil-} is the foil thickness (15 mm Cu for Li-ion, 10 □m Al for Na-ion) and d_{foil-} its density. The last factor accounts for the fact that the foils are coated on both sides except for the two outer layers.

The separator weight m_{sep} is calculated as follows:

$$m_{sep} = A \cdot e_{sep} \cdot d_{sep} \cdot n$$

where e_{sep} and d_{sep} are the separator thickness and density, respectively.

The electrolyte weight m_{el} is calculated as follows:

$$m_{el} = A \cdot [(e_+ + e_-) \cdot P + e_{sep} \cdot P_{sep}] \cdot n$$

where P_{sep} is the separator's thickness.

Finally, the number of stacks has been determined as follows, after rounding to the closest even integer value:

$$n \approx \frac{e_{cell}^{target} - e_{foil-}}{e_+ + e_- + e_{sep} + \frac{e_{foil+} + e_{foil-}}{2}}$$

where e_{cell}^{target} is the target value for the total cell thickness (1 cm for all Li-ion and Na-ion cells). The actual cell thickness e_{cell} is then calculated as:

$$e_{cell} = n\left(e_+ + e_- + e_{sep} + \frac{e_{foil+} + e_{foil-}}{2}\right) + e_{foil-}$$

According to a reference calculation we performed using the BatPac4.0 software for a NMC111-g Li-ion pouch cell using default values for all parameters (results for a 300 Wh EV battery pack, see table S7),[20] the contact tabs and pouch envelop account for 11.9% extra volume and 5.3% additional weight compared to the nude cell, respectively, and the energy density at pack level is found about 40% lower per volume unit and 20 % lower per mass unit compared to the cell

results (including tabs and envelop). This gives an indication on how to extrapolate to the pack level the results of the calculation of the present review at cell level using the above equations. In addition to this reference NMC111-g simulation using BatPac4.0 with default values, a second simulation using BatPac4.0 has been performed limiting the cathode thickness to 65 □m, all other parameters being unchanged. As can be seen in Table S7 these results for NMC111-g using BatPac4.0 with 65 □m matches very well the results of the present calculations using the equations above, which validates the present method.

Table S3. Properties of the non-active materials.

Material	Thickness (µm)	Porosity (%)	Density (g/cm^3)
Binder (PVDF)			1.78
Carbon black			1.77
Separator (Celgard A273 monoPP)	16	40	0.86
Electrolyte (LP30)			1.3
Al foil	15		2.79
Cu foil	10		8.96

Table S4. Active materials properties for the positive electrode of Li-ion and Na-ion cells. Capacity and average oxidation potential for Li-ion materials are from the references indicated in the table, and those for Na-ion materials have been calculated from the discharge curves presented in Figure 2 of the main text. The densities have been calculated from the crystallographic data whenever available, the related references are indicated in the table. Electrode densities have been calculated assuming 30% porosity and 90:5:5 active material/Binder/Carbon black electrode composition.

Cathode material	Short name	Capacity (mA h / g)	Average oxidation potential (V)	Material density (g / cm^3)	Electrode density (g / cm^3)
$LiNi_{0.8}Mn_{0.1}Co_{0.1}O_2$	NMC811	200 [21]	3.8 [21]	4.87 [23]	2.90
$LiNi_{1/3}Mn_{1/3}Co_{1/3}O_2$	NMC111	160 [21]	3.75 [21]	4.77 [24]	2.86
$LiCoO_2$	LCO	140 [19]	3.85 [19]	4.93 [25]	2.93
Li_2MnO_3	LMO	120 [21]	4.0 [21]	4.01 [25]	2.49
$LiFePO_4$	LFP	165 [21]	3.45 [21]	3.46 [25]	2.21
$LiFePO_4$-C(5%)	LFP-C	160	3.45	3.31 [a]	2.13
O3-$NaNi_{0.45}Zn_{0.05}Mn_{0.4}Ti_{0.1}O_2$	O3	172	3.31	4.53 [26]	2.74
P2-$Na_{0.67}Cu_{0.14}Fe_{0.2}Mn_{0.66}O_2$	P2	193	2.71	4.15 [27]	2.56
P2-$Na_{0.67}Cu_{0.14}Fe_{0.2}Mn_{0.66}O_2$ (x <= 2/3)	P2-CE	141	2.99	4.15 [27]	2.56
$Na_3V_2(PO_4)_3$	NVP	103	3.32	3.04 [25]	1.99
$Na_3V_2(PO_4)_2F_3$	NVPF	118	3.91	3.16 [28]	2.05
$Na_xM[Fe(CN)_6]_y.zH_2O$	PBA	144	3.35	1.96 [29]	1.36

[a]: Calculated from $LiFePO_4$ assuming a density of 1.8 g/cm^3 for the 5% carbon coating.

Table S5. Active materials properties for the negative electrode of Li-ion and Na-ion cells. Capacity and average oxidation potential for graphite vs Li^+/Li are from the reference indicated in the table, and those for Na-ion materials have been calculated from the discharge curves presented in Figure 3 of the main text, except for the soft carbon which is extracted from ref. [30] The densities have been calculated from the crystallographic data whenever available, the related references are indicated in the table. When the active material is embedded in a carbon matrix (TiO_2/C, Sb/C, MoS_2/C & Sb_2O_3/C), the density has been calculated taking into account the carbon matrix, whose density has been estimated as 1.91 g/cm^3 for rGO,[31] 1.8 g/cm^3 in the case of Sb/C and Sn/C. Electrode densities have then been calculated assuming 30% porosity and 90:5:5 active material/Binder/Carbon black electrode composition.

Anode material	Short name	Capacity (mA h / g)	Average reduction potential (V)	Material density (g / cm^3)	Electrode density (g / cm^3)
Graphite (vs Li^+/Li)	g	350 [19]	0.1 [19]	2.26 [32]	1.54
Na-solvent co-intercalated graphite	ci-g	97	1.0	2.26 [32]	1.54
Hard carbon	HC	322	0.43	1.80 [a]	1.26
Soft carbon	SC	200 [30]	0.6 [30]	2.0 [a]	1.38
TiO_2-rGO	TiO_2/C	266	1.23	2.95 [33]	1.96
$Na_2Ti_3O_7$	NTO	167	0.97	3.44 [34]	2.20
P/rGO	P/C	1043	0.79	2.10	1.44
Sb/C	Sb/C	428	0.80	3.69	2.33
Sn NDS@PNC	Sn/C	625	0.74	3.18	2.06
MoS_2/rGO	MoS_2/C	533	1.54	3.34	2.15
Sb_2O_3/rGO	Sb_2O_3/C	465	1.15	3.68	2.33

[a]: He pycnometer measurement by the authors on sugar hard carbon pyrolyzed at 1050 ºC and PVC soft carbon pyrolyzed at 800ºC

Table S6. Simulated cell parameters for 65 µm thick positive electrode coating.

Active materials		Loading (mA h / cm^2)	Anode thickness (µm)	Cell weight (kg/L)	Cell thickness (cm)	n stack	Areal weight (g / cm^2)			
+	-						El. & sep.	AM	Binder & CB	CCs
Li-ion cells										
NMC811	g	3.71	68.9	2.63	1.01	62	6.88	26.26	2.92	6.72
NMC111	g	2.97	55.1	2.70	1.01	68	6.34	24.35	2.71	6.70
LCO	g	2.67	49.5	2.76	1.00	70	6.12	24.00	2.67	6.70
LFP	g	2.38	44.1	2.45	0.99	72	5.91	19.06	2.12	6.70
LFP-C	g	2.22	41.1	2.42	1.00	74	5.79	18.16	2.02	6.69
LMO	g	1.94	36.1	2.62	1.01	78	5.59	19.58	2.18	6.69
Na-ion cells										
P2	HC	3.21	79.3	2.17	0.98	56	7.28	23.97	2.66	4.26
P2-CE	HC	2.34	57.8	2.25	0.99	64	6.44	21.54	2.39	4.25
NVP	HC	1.32	32.6	2.07	1.00	78	5.46	15.32	1.70	4.24
NVPF	HC	1.57	38.8	2.09	1.00	74	5.70	16.41	1.82	4.24
PBA	HC	1.27	31.4	1.76	1.00	78	5.41	11.50	1.28	4.24
O3	HC	3.07	75.6	2.25	1.00	58	7.14	24.62	2.74	4.26
O3	SC	3.07	110.9	2.22	0.99	48	8.51	29.85	3.32	4.27
O3	TiO_2/C	3.07	58.8	2.59	0.99	64	6.48	26.42	2.94	4.25
O3	NTO	3.07	83.1	2.67	1.00	56	7.43	32.54	3.62	4.26
O3	ci-g	3.07	206.0	2.19	1.03	34	12.2	44.61	4.96	4.31
O3	P/C	3.07	20.4	2.57	1.00	86	4.98	18.70	2.08	4.23
O3	Sb/C	3.07	30.7	2.73	0.99	78	5.39	22.50	2.50	4.24
O3	Sn/C	3.07	23.8	2.68	1.01	84	5.12	20.47	2.27	4.23
O3	MoS_2/C	3.07	26.8	2.69	1.01	82	5.23	21.23	2.36	4.24
O3	Sb_2O_3/C	3.07	28.3	2.73	1.00	80	5.29	21.99	2.44	4.24

Table S7. Comparison of the calculation of the energy density for a NMC111-g cell of the present work, compared to reference calculations performed using ANL's BatPac software tool [20] for a cell within an 300kW battery pack optimized for EV application with water-glycol cooling. "BatPac default (120 m cathode coating)" corresponds to the results using all parameters set to default, for which the cathode coating thickness is 120 m, and "BatPac default (65 m cathode coating)" corresponds to the results using all parameters set to default except for the cathode coating thickness that is set to 65m.

Method	Energy_Cell (W h / L)	Energy_Cell (W h / kg)	Energy_Pack (W h / L)	Energy_Pack (W h / kg)
Present work (65 m cathode coating)	656	243	NA	NA
BatPac default (120 m cathode coating)	661	262	385	209
BatPac default (65 m cathode coating)	614	240	362	193

Table S8. Current status of Li-ion and Na-ion technology in 2020 and mid-term targets for 2030 compared to the performance targets set by the EU Integrated Strategic Energy Technology Plan (SET-Plan) Action 7 for 2030. [35]

SET Plan targets at cell level for 2020 and current status										
	(TRL)	***Energy density***		***Power Density***		***Cycle Life***		***Cost***	***Recycling / Battery take back***	***Second life***
	Level	*[Wh kg^{-1}]*	*[Wh L^{-1}]*	*[W kg^{-1}]*	*[W L^{-1}]*	*Automotive*	*Stationary*	*[€/KWh/cycle] or [€/KWh]*	*Rate / %*	*Status*
EU SET plan 2020 [36]	TRL 9	350	750	700	1500	1000 (*to 80% DOD*)	3000-5000 15 years	0.1 *€/KWh/cycle* (in 2022 for stationary) 90 *€/KWh (in 2022 for automotive)*	70 %	Developed
Li-ion (current status 2020)	TRL9	~150-250 [37, 38]	200-[37]-600[38]	340-600 (for BEV [37])	800 [39]	1000	5000 10 years	~100 €/kWh [40] 220-300 €/kWh (LFP cell) [41] 140-290 €/kWh (NMC-cell)[41]	--	Under development
Na-ion (current status 2020)	TRL7	90 [11]-140 [7,42]	150-210 [7]	--*	--*	2000 [7,43] - 3750[11]	3000	~0.09-0.03 *€/KWh/cycle* (considering 10-30% cost cut) 220[41] €/kWh	--	Not developed
SET Plan targets at cell level for 2030										
	(TRL)	***Energy density***		***Power Density***		***Cycle Life***		***Cost***	***Recycling / Battery take back***	***Second life***
	Level	*[Wh kg^{-1}]*	*[Wh L^{-1}]*	*[W kg^{-1}]*	*[W L^{-1}]*	*BEV*	*Stationary*	*[€/KWh/cycle] or [€/KWh]*	*Rate / %*	*Status*
EU SET plan 2030 [36]	TRL 9	>400	>750	>700	>1500	2000 (to 80% DoD)	10000 20 years	0.05 €/kWh/cycle < 100 €/kWh	85%	Fully established
Na-ion 2030 (envisioned values)	TRL9	>250	>400	>300	600	5000 (light vehicles)	10000	0.025 €/kWh/cycle ~100 €/kWh	85%	Developed

* Power performance is generally assessed through rate capability tests. A range of different current densities and cycling conditions (different charge and discharge currents, temperature) are reported in literature making a fair comparison very challenging.

It is worth mentioning that the KPIs for 2030 are based on several assumptions. The cost estimation can indeed be affected by many parameters not considered in this work such as geographical constrains, political policies and mid-term availability of raw materials. It is assumed that the rate of battery take for recycling will follow the same trend as for the Li-ion technology and second life will be also established (assuming mass production of NIBs will reach considerable values in the next years).

References:

[1] P. Hartmann, C.L. Bender, M. Vračar, A.K. Dürr, A. Garsuch, J. Janek, P. Adelhelm, A rechargeable room-temperature sodium superoxide (NaO2) battery, Nat. Mater. 12 (2013) 228–232. https://doi.org/10.1038/nmat3486.

[2] N. Wang, Y. Wang, Z. Bai, Z. Fang, X. Zhang, Z. Xu, Y. Ding, X. Xu, Y. Du, S. Dou, G. Yu, High-performance room-temperature sodium-sulfur battery enabled by electrocatalytic sodium polysulfides full conversion, Energy Environ. Sci. 13 (2020) 562–570. https://doi.org/10.1039/c9ee03251g.

[3] S. Mariyappan, Q. Wang, J.M. Tarascon, Will Sodium Layered Oxides Ever Be Competitive for Sodium Ion Battery Applications?, J. Electrochem. Soc. 165 (2018) A3714–A3722. https://doi.org/10.1149/2.0201816jes.

[4] J. Song, K. Wang, J. Zheng, M.H. Engelhard, B. Xiao, E. Hu, Z. Zhu, C. Wang, M. Sui, Y. Lin, D. Reed, V.L. Sprenkle, P. Yan, X. Li, Controlling Surface Phase Transition and Chemical Reactivity of O3-Layered Metal Oxide Cathodes for High-Performance Na-Ion Batteries, ACS Energy Lett. (2020) 1718–1725. https://doi.org/10.1021/acsenergylett.0c00700.

[5] S.-M. Oh, P. Oh, S.-O. Kim, A. Manthiram, A High-Performance Sodium-Ion Full Cell with a Layered Oxide Cathode and a Phosphorous-Based Composite Anode, J. Electrochem. Soc. 164 (2016) A321–A326. https://doi.org/10.1149/2.0931702jes.

[6] I. Hasa, S. Passerini, J. Hassoun, A rechargeable sodium-ion battery using a nanostructured Sb–C anode and P2-type layered Na0.6Ni0.22Fe0.11Mn0.66O2 cathode, RSC Adv. 5 (2015) 48928–48934. https://doi.org/10.1039/C5RA06336A.

[7] A. Bauer, J. Song, S. Vail, W. Pan, J. Barker, Y. Lu, The Scale-up and Commercialization of Nonaqueous Na-Ion Battery Technologies, Adv. Energy Mater. 8 (2018) 1–13. https://doi.org/10.1002/aenm.201702869.

[8] C. Zhao, F. Ding, Y. Lu, L. Chen, Y.-S. Hu, High-Entropy Layered Oxide Cathodes for Sodium-Ion Batteries, Angew. Chemie Int. Ed. 59 (2020) 264–269. https://doi.org/10.1002/anie.201912171.

[9] Y. Xie, G.-L. Xu, H. Che, H. Wang, K. Yang, X. Yang, F. Guo, Y. Ren, Z. Chen, K. Amine, Z.-F. Ma, Probing Thermal and Chemical Stability of NaxNi1/3Fe1/3Mn1/3O2 Cathode Material toward Safe Sodium-Ion Batteries, Chem. Mater. 30 (2018) 4909–4918. https://doi.org/10.1021/acs.chemmater.8b00047.

[10] J. Deng, W.-B. Luo, X. Lu, Q. Yao, Z. Wang, H.-K. Liu, H. Zhou, S.-X. Dou, High Energy Density Sodium-Ion Battery with Industrially Feasible and Air-Stable O3-Type Layered Oxide Cathode, Adv. Energy Mater. 8 (2018) 1701610. https://doi.org/doi:10.1002/aenm.201701610.

[11] T. Broux, F. Fauth, N. Hall, Y. Chatillon, M. Bianchini, T. Bamine, J.B. Leriche, E. Suard, D.

Carlier, Y. Reynier, L. Simonin, C. Masquelier, L. Croguennec, High Rate Performance for Carbon-Coated Na3V2(PO4)2F3 in Na-Ion Batteries, Small Methods. 3 (2019). https://doi.org/10.1002/smtd.201800215.

[12] S. Saxena, C. Hendricks, M. Pecht, Cycle life testing and modeling of graphite/LiCoO2 cells under different state of charge ranges, J. Power Sources. 327 (2016) 394–400. https://doi.org/10.1016/j.jpowsour.2016.07.057.

[13] Y. Fang, Q. Liu, L. Xiao, X. Ai, H. Yang, Y. Cao, High-Performance Olivine NaFePO4 Microsphere Cathode Synthesized by Aqueous Electrochemical Displacement Method for Sodium Ion Batteries, ACS Appl. Mater. Interfaces. 7 (2015) 17977–17984. https://doi.org/10.1021/acsami.5b04691.

[14] G. Longoni, J.E. Wang, Y.H. Jung, D.K. Kim, C.M. Mari, R. Ruffo, The Na2FeP2O7-carbon nanotubes composite as high rate cathode material for sodium ion batteries, J. Power Sources. 302 (2016) 61–69. https://doi.org/10.1016/j.jpowsour.2015.10.033.

[15] T. Yuan, Y. Wang, J. Zhang, X. Pu, X. Ai, Z. Chen, H. Yang, Y. Cao, 3D graphene decorated Na4Fe3(PO4)2(P2O7) microspheres as low-cost and high-performance cathode materials for sodium-ion batteries, Nano Energy. 56 (2019) 160–168. https://doi.org/10.1016/j.nanoen.2018.11.011.

[16] X. Liu, L. Tang, Q. Xu, H. Liu, Y.G. Wang, Ultrafast and ultrastable high voltage cathode of Na2+2xFe2-x(SO4)3 microsphere scaffolded by graphene for sodium ion batteries, Electrochim. Acta. 296 (2019) 345–354. https://doi.org/10.1016/j.electacta.2018.11.064.

[17] M. Law, V. Ramar, P. Balaya, Na2MnSiO4 as an attractive high capacity cathode material for sodium-ion battery, J. Power Sources. 359 (2017) 277–284. https://doi.org/10.1016/j.jpowsour.2017.05.069.

[18] Z. Jian, W. Han, X. Lu, H. Yang, Y.S. Hu, J. Zhou, Z. Zhou, J. Li, W. Chen, D. Chen, L. Chen, Superior electrochemical performance and storage mechanism of Na 3 V 2 (PO 4) 3 cathode for room-temperature sodium-ion batteries, Adv. Energy Mater. 3 (2013) 156–160. https://doi.org/10.1002/aenm.201200558.

[19] J.W. Choi, D. Aurbach, Promise and reality of post-lithium-ion batteries with high energy densities, Nat. Rev. Mater. 1 (2016) 1–16. https://doi.org/10.1038/natrevmats.2016.13.

[20] BatPaC Model Software | Argonne National Laboratory, (n.d.). https://www.anl.gov/cse/batpac-model-software (accessed June 10, 2020).

[21] M. Wentker, M. Greenwood, J. Leker, A Bottom-Up Approach to Lithium-Ion Battery Cost Modeling with a Focus on Cathode Active Materials, Energies. 12 (2019) 504. https://doi.org/10.3390/en12030504.

[22] Lain, Brandon, Kendrick, Design Strategies for High Power vs. High Energy Lithium Ion Cells, Batteries. 5 (2019) 64. https://doi.org/10.3390/batteries5040064.

[23] J. Sturm, A. Rheinfeld, I. Zilberman, F.B. Spingler, S. Kosch, F. Frie, A. Jossen, Modeling and simulation of inhomogeneities in a 18650 nickel-rich, silicon-graphite lithium-ion cell during fast charging, J. Power Sources. 412 (2019) 204–223. https://doi.org/10.1016/j.jpowsour.2018.11.043.

[24] E.J. Cheng, K. Hong, N.J. Taylor, H. Choe, J. Wolfenstine, J. Sakamoto, Mechanical and physical properties of LiNi0.33Mn0.33Co0.33O2 (NMC), J. Eur. Ceram. Soc. 37 (2017)

3213–3217. https://doi.org/10.1016/j.jeurceramsoc.2017.03.048.

[25] Materials Project, (n.d.). https://materialsproject.org/ (accessed June 10, 2020).

[26] S. Mariyappan, T. Marchandier, F. Rabuel, A. Iadecola, G. Rousse, A. V Morozov, A.M. Abakumov, J.-M. Tarascon, The Role of Divalent (Zn2+/Mg2+/Cu2+) Substituents in Achieving Full Capacity of Sodium Layered Oxides for Na-Ion Battery Applications, Chem. Mater. 32 (2020) 1657–1666. https://doi.org/10.1021/acs.chemmater.9b05205.

[27] E. Talaie, S.Y. Kim, N. Chen, L.F. Nazar, Structural Evolution and Redox Processes Involved in the Electrochemical Cycling of P2-Na0.67[Mn0.66Fe0.20Cu0.14]O2, Chem. Mater. 29 (2017) 6684–6697. https://doi.org/10.1021/acs.chemmater.7b01146.

[28] M. Bianchini, N. Brisset, F. Fauth, F. Weill, E. Elkaim, E. Suard, C. Masquelier, L. Croguennec, Na3V2(PO4)2F3 revisited: A high-resolution diffraction study, Chem. Mater. 26 (2014) 4238–4247. https://doi.org/10.1021/cm501644g.

[29] K. Hurlbutt, S. Wheeler, I. Capone, M. Pasta, Prussian Blue Analogs as Battery Materials, Joule. 2 (2018) 1950–1960. https://doi.org/10.1016/j.joule.2018.07.017.

[30] D. Saurel, B. Orayech, B. Xiao, D. Carriazo, X. Li, T. Rojo, From Charge Storage Mechanism to Performance: A Roadmap toward High Specific Energy Sodium-Ion Batteries through Carbon Anode Optimization, Adv. Energy Mater. 8 (2018) 1–33. https://doi.org/10.1002/aenm.201703268.

[31] Reduced Graphene Oxide (1 Gram) – Graphenea, (n.d.). https://www.graphenea.com/products/reduced-graphene-oxide-1-gram (accessed June 10, 2020).

[32] L. Boulet-Roblin, D. Sheptyakov, P. Borel, C. Tessier, P. Novák, C. Villevieille, Crystal structure evolution: Via operando neutron diffraction during long-term cycling of a customized 5 v full Li-ion cylindrical cell LiNi0.5Mn1.5O4 vs. graphite, J. Mater. Chem. A. 5 (2017) 25574–25582. https://doi.org/10.1039/c7ta07917f.

[33] Refinement of the structure of anatase at several temperatures in: Zeitschrift für Kristallographie - Crystalline Materials Volume 136 Issue 1-6 (1972), (n.d.). https://www.degruyter.com/view/journals/zkri/136/1-6/article-p273.xml (accessed June 10, 2020).

[34] P. Senguttuvan, G. Rousse, V. Seznec, J.M. Tarascon, M.R. Palacín, Na2Ti3O7: Lowest voltage ever reported oxide insertion electrode for sodium ion batteries, Chem. Mater. 23 (2011) 4109–4111. https://doi.org/10.1021/cm202076g.

[35] (No Title), (n.d.). https://setis.ec.europa.eu/system/files/integrated_set-plan/action7_declaration_of_intent_0.pdf (accessed May 31, 2020).

[36] “Become competitive in the global battery sector to drive e-mobility and stationary storage forward” Integrated SET-Plan Action 7, Implementation Plan., 2016.

[37] D. Andre, H. Hain, P. Lamp, F. Maglia, B. Stiaszny, Future high-energy density anode materials from an automotive application perspective, J. Mater. Chem. A. 5 (2017) 17174–17198.

[38] Y.E. Durmus, H. Zhang, F. Baakes, G. Desmaizieres, H. Hayun, L. Yang, M. Kolek, V. Küpers, J. Janek, D. Mandler, S. Passerini, Y. Ein-Eli, Side by Side Battery Technologies with Lithium-Ion Based Batteries, Adv. Energy Mater. 10 (2020). https://doi.org/10.1002/aenm.202000089.

[39] G.J. May, A. Davidson, B. Monahov, Lead batteries for utility energy storage: A review, J. Energy Storage. 15 (2018) 145–157. https://doi.org/10.1016/j.est.2017.11.008.

[40] https://cleantechnica.com/2019/12/04/powering-the-ev-revolution-battery-packs-now-at-156-kwh-13-lower-than-2018-finds-bnef/, (n.d.).

[41] J.F. Peters, A.P. Cruz, M. Weil, Exploring the economic potential of sodium-ion batteries, Batteries. 5 (2019). https://doi.org/10.3390/batteries5010010.

[42] J. Barker, R.J. Heap, N. Roche, C. Tan, R. Sayers, J. Whitley, Y. Lui, Commercialization of Faradion ' s High Energy Faradion : Introduction, (n.d.).

[43] http://www.hinabattery.com/en/index.php?catid=12, (n.d.).